Article

Importance of Length and Sequence Order on Magnesium Binding to Surface-Bound Oligonucleotides Studied by Second Harmonic Generation and Atomic Force Microscopy

Joseph G. Holland and Franz M. Geiger*

Department of Chemistry, Northwestern University, 2145 Sheridan Road, Evanston, Illinois 60208, United States

Ⓢ *Supporting Information*

ABSTRACT: The binding of magnesium ions to surface-bound single-stranded oligonucleotides was studied under aqueous conditions using second harmonic generation (SHG) and atomic force microscopy (AFM). The effect of strand length on the number of Mg(II) ions bound and their free binding energy was examined for 5-, 10-, 15-, and 20-mers of adenine and guanine at pH 7, 298 K, and 10 mM NaCl. The binding free energies for adenine and guanine sequences were calculated to be −32.1(4) and −35.6(2) kJ/mol, respectively, and invariant with strand length. Furthermore, the ion density for adenine oligonucleotides did not change as strand length increased, with an average value of 2(1) ions/strand. In sharp contrast, guanine oligonucleotides displayed a linear relationship between strand length and ion density, suggesting that cooperativity is important. This data gives predictive capabilities for mixed strands of various lengths, which we exploit for 20-mers of adenines and guanines. In addition, the role sequence order plays in strands of hetero-oligonucleotides was examined for $5'-A_{10}G_{10}-3'$, $5'-(AG)_{10}-3'$, and $5'-G_{10}A_{10}-3'$ (here the -3′ end is chemically modified to bind to the surface). Although the free energy of binding is the same for these three strands (averaged to be −33.3(4) kJ/mol), the total ion density increases when several guanine residues are close to the 3′ end (and thus close to the solid support substrate). To further understand these results, we analyzed the height profiles of the functionalized surfaces with tapping-mode atomic force microscopy (AFM). When comparing the average surface height profiles of the oligonucleotide surfaces pre- and post- Mg(II) binding, a positive correlation was found between ion density and the subsequent height decrease following Mg(II) binding, which we attribute to reductions in Coulomb repulsion and strand collapse once a critical number of Mg(II) ions are bound to the strand.
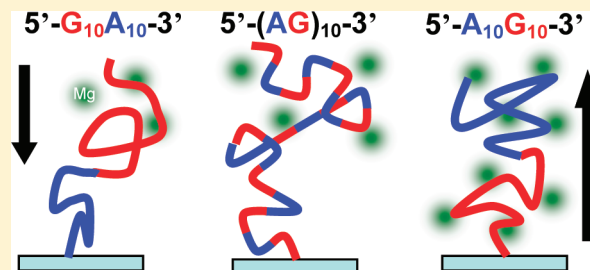
I. INTRODUCTION

Metal ions play some of the most fundamental roles in determining nucleic acid properties. Divalent metal cations are known to be essential to nucleic acid structure,[1−6] replication, and transcription[7−10] and even serve as the target molecules for some biodiagnostic sensors.[11−14] Short sequences of DNA, commonly referred to as oligonucleotides, are being increasingly incorporated into surface-based biosensors[13,15−18] and nanotemplates[19−22] based upon their propensity to selectively and strongly bind to a wide range of target analytes. In recent years, great progress has been made in developing aptamers for use as surface-based sensors.[23−26]

In these diverse systems, DNA sequences are often immobilized via one end, leaving the other end free to interact with the target in the aqueous phase. Unfortunately, from a molecular perspective, these surface-based systems are often complex and difficult to study in a surface-specific fashion without utilizing labels extrinsic to the system. Thus, from the standpoint of understanding fundamental oligonucleotide function, it is desirable to develop and advance a nondestructive and label-free approach to studying surface-bound oligonucleotides. Building upon our recent successes in understanding and quantifying similar surface-based systems under aqueous

conditions,[27−34] this work provides such an approach using the Eisenthal $\chi^{(3)}$ technique[35,36] as well as atomic force microscopy (AFM).

Here, we study Mg(II) because (a) it is ubiquitous in the chemistry of DNA,[37−40] (b) it has ideal bulk speciation under the conditions of interest, and (c) the studies described represent a clear and necessary continuity from those we have previously reported.[27,41,42] While many studies have characterized the binding properties of magnesium to DNA in bulk solution,[43−57] at this time, there is no known way of correctly predicting Mg(II) ion densities and total binding free energies from first principles for interfacial environments. Here, we quantify the free energy of binding and ion density (ions/ strand) of divalent magnesium ions to varied length homo-oligomers and mixed strands covalently attached to fused silica/ water interfaces maintained at pH 7 and 10 mM NaCl concentration. Tapping mode AFM was used to provide a macroscopic analysis of the nanoscale properties of surface topography under aqueous conditions identical to those used in
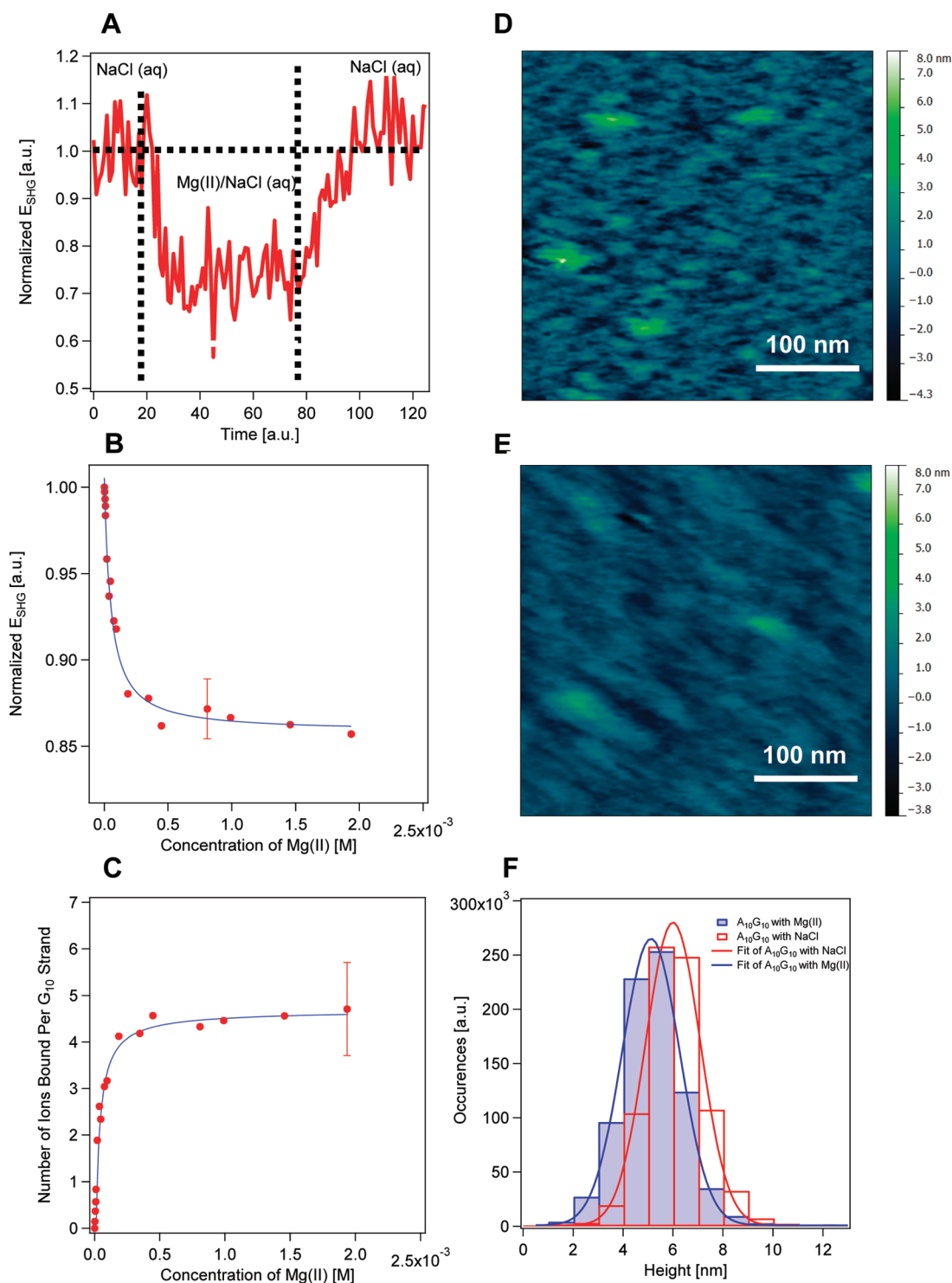
Figure 1. (A) On/Off trace for Mg(II) binding to the G_{10}-functionalized fused silica which illustrates reversibility of binding for a bulk concentration of 1.4 mM $MgCl_2$. SHG E-field as a function of time for a flow rate of 1 mL/s. (B) Adsorption isotherm for Mg(II) at the G_{10}-functionalized fused silica/water interface carried out at pH 7 and in the presence of 10 mM NaCl. All adsorption experiments were collected in duplicate or triplicate. The solid line is the fit of the data using eq 2. (C) Loading curve for Mg(II) to G_{10} strands as a function of bulk $MgCl_2$ concentration, calculated using eq 3. (D) $A_{10}G_{10}$ functionalized surface imaged using tapping mode AFM under aqueous conditions at pH 7, 298 K, and 10 mM NaCl. (E) $A_{10}G_{10}$ functionalized surface imaged using tapping mode AFM under aqueous conditions at pH 7, 10 mM NaCl, 298 K, and 3 mM $MgCl_2$. (F) Example histogram analysis of the height profiles of the $A_{10}G_{10}$ functionalized surface pre- and post-Mg(II) binding.

the nonlinear optical studies. By combining two independent experiments, we hope to further elucidate the interactions of ions with oligonucleotides on surfaces. Homo-oligomers of guanine and adenine were chosen based on our previous

reports that identified those two nucleobases as the strongest and weakest binders with ΔG_{bind} values of −35.9(4) and −31(1) kJ/mol, respectively,[58] but neglected the role of sequence order in predictions of binding free energies, even

though this role may be important for synergistic effects. Additionally, these nucleobases represent the extremes of ion binding within the sequence space surveyed, with 20-mers of guanine and adenine binding 11(2) and 3(2) ions/strand, respectively.[58] The quantitative data presented here will serve as the foundation of a surface-specific database of nucleotide/analyte interactions and be useful as an experimental benchmark for computational studies.

II. EXPERIMENTAL SECTION

A. Surface Preparation, Functionalization, and Materials. All of the experiments described herein use either fused silica hemispheres (ISP Optics) or heavily doped Si wafers with 300 nm of thermally grown silicon dioxide as the substrate material. Prior to functionalization, the fused silica hemisphere substrates were cleaned by exposing them to NoChromix solution (Godax Laboratories) for 1 h. Although Si/SiO$_2$ wafers were not subjected to NoChromix cleaning, all subsequent cleaning and functionalization procedures were identical to those for the hemispheres. After thoroughly rinsing the substrates with Millipore water (18.2 MΩ), they were submerged in a beaker of methanol and sonicated for 10 min. The substrates were then placed in an oven at 100 °C for 30 min. Lastly, the substrates were plasma cleaned (Harrick Plasma) for 3 min on the highest instrument setting. The substrates were then functionalized with an N-hydroxysuccinimide linker using our previously reported method.[58−60] The oligonucleotides (Integrated DNA Technologies) used in this work had the following sequences: A$_5$: 5′-AAA AA/3AmMO/-3′; A$_{10}$: 5′-AAA AAA AAA A/3AmMO/-3′; A$_{15}$: 5′-AAA AAA AAA AAA AAA/3AmMO/-3′; A$_{21}$: 5′-AAA AAA AAA AAA AAA AAA AAA/3AmMO/-3′; G$_5$: 5′-GGG GG/3AmMO/-3′; G$_{10}$: 5′-GGG GGG GGG G/3AmMO/-3′; G$_{15}$: 5′-GGG GGG GGG GGG GGG/3AmMO/-3′; G$_{20}$: 5′-GGG GGG GGG GGG GGG GGG GG/3AmMO/-3′; G$_{10}$A$_{10}$: 5′-GGG GGG GGG GAA AAA AAA AA/3AmMO/-3′; A$_{10}$G$_{10}$: 5′-AAA AAA AAA AGG GGG GGG GG/3AmMO/-3′; (AG)$_{10}$: 5′-(AG)$_{10}$/3AmMO/-3′. The strands were covalently attached to the silica surface via amide bond formation that occurs through the /3AmMO/-3′ modification and the N-hydroxysuccinimide linker.[27,41,42,59,60] Aqueous solutions were prepared using Millipore water and adjusted to pH 7 by the addition of dilute HCl (E.M.D., ACS grade) and dilute NaOH (Sigma-Aldrich, 99.99%). The aqueous solutions of the 0.1 M MgCl$_2$ stock were prepared by using MgCl$_2$(H$_2$O)$_6$ (Sigma-Aldrich, 99.99%). Background electrolyte solution for all experiments was 10 mM NaCl (VWR, 99%). The pH meter (Thermo Fisher) used in this study was calibrated daily. All metal concentrations were quantified using calibrated inductively coupled plasma atomic emission spectroscopy (ICP-AES, Varian).

B. Second Harmonic Generation. Pertinent background information on both the laser and flow systems can be found in our previous work.[41,61−64] The SHG experiments described in this work were performed using a regeneratively amplified Ti:sapphire laser (Hurricane, Spectra-Physics) which pumped an optical parametric amplifier (OPA-CF, Spectra-Physics) at a 1 kHz repetition rate. Using the OPA, the incident beam was tuned to the desired wavelength of 600 ± 15 nm and then attenuated to 0.55 ± 0.05 μJ using a variable density filter. The fundamental beam at frequency ω was focused on the oligonucleotide-functionalized fused silica/water interface, which generated the second harmonic beam at frequency 2ω. The reflected photons due to the fundamental were selectively

removed using a UV-grade Schott filter, and the second harmonic photons were directed through a monochromator set to 2ω into a photomultiplier tube, amplified, and counted using single photon counting techniques. Detailed explanations of the data analysis, the interpretation of the adsorption/desorption ("on/off") traces, and a full sensitivity analysis of the models applied to interpret our data can be found in our previously published work.[36,41,61−67] All of the experiments described in this work were performed at pH 7, 10 mM NaCl, with a flow rate of ∼1 mL/s, for (a) comparison to our previously published work on surface-bound single-stranded oligonucleotide and (b) to accommodate our modified Gouy−Chapman fitting equation. The adsorption isotherms were performed in either duplicate or triplicate. All of the adsorption isotherms can be found in the Supporting Information.

C. Adsorption Isotherms. SHG experiments were performed to assess the binding of Mg(II) to adenine and guanine 5−20-mers and mixed 20-mer strands of guanine and adenine. The second harmonic E-field (E_{SHG}), which equals the square root of the second harmonic intensity (I_{SHG}), is produced in the interfacial region where symmetry is broken. The I_{SHG} is proportional to the polarization of the interface ($P_{2\omega}$), which can be defined as shown in eq 1.

$$\sqrt{I_{SHG}} = E_{SHG} \propto P_{2\omega} = A + B\Phi_0 \tag{1}$$

In this equation, A and B represent the product of the incident electric fields with the second- or third-order nonlinear susceptibility of the system, respectively, and are assumed to be constant.[36,68] Importantly, eq 1 is insensitive to changes in A and B that are relevant in this work.[58] Therefore, E_{SHG} is directly related to the initial interfacial potential (Φ_0). Initially, single-stranded oligonucleotides exhibit a high Φ_0, and thus a high E_{SHG}, due to the presence of the negatively charged phosphate backbone. When Mg(II) ions are introduced to the system, they bind to the oligonucleotides and thus decrease both Φ_0 and E_{SHG}. It should be noted that all oligonucleotide/divalent metal interactions studied to date using SHG have proven to exhibit reversible binding. Based on these principles, SHG $\chi^{(3)}$ isotherms (Figure 1b) were produced by collecting on/off traces (Figure 1a) for a range of bulk Mg(II) concentrations (10^{-6}−10^{-3} M). Comprehensive experimental details as well as additional background on second harmonic generation can be found in previously published work on Mg(II)/oligonucleotide binding.[41,42] Adsorption isotherms for all experiments presented in this work may be found in the Supporting Information (Figures S1−S10).

All E_{SHG} values were normalized by calculating the square root of the I_{SHG} in the presence of Mg(II) divided by the square root of the average I_{SHG} obtained while flowing a 10 mM NaCl solution across the interfaces before and after Mg(II) flow. Control studies verified that the changes in E_{SHG} are not merely the result of increasing ionic strength but are specifically due to analyte binding.[36,62] All isotherms presented here were fit by substituting the Langmuir isotherm-modified Gouy−Chapman equation into eq 1 to yield eq 2.

$$E_{SHG} = A + B \sinh^{-1}\left[\sigma_0 + \sigma_m\left(\frac{K_{bind}[M]}{1 + K_{bind}[M]}\right)\right.$$
$$\left.\frac{30.19 \text{ M}^{1/2} \text{ m}^2 \text{ C}^{-1}}{\sqrt{C_{elec}}}\right] \tag{2}$$

6304

dx.doi.org/10.1021/jp301573g | J. Phys. Chem. B 2012, 116, 6302−6310

In eq 2, σ_0 is the initial surface charge density of the surface-bound oligonucleotide in the absence of Mg(II) which scales with the oligonucleotide length, σ_m is the maximum surface charge density due to bound Mg(II), [M] is the concentration of Mg^{2+} in bulk solution, C_{elec} is the sum of both the concentration of [NaCl] and [Mg(II)], K_{bind} is the measured binding constant, and $30.19 \; M^{1/2} \; m^2 \; C^{-1}$ is the product of the natural constants in the Gouy−Chapman equation. Use of the Gouy−Chapman theory for the analysis of divalent metal binding to oligonucleotide-functionalized surfaces, including the treatment of C_{elec} as the sum of the Mg^{2+} and NaCl concentration vs just the NaCl concentration, has been discussed in our previous work.[41,69,70] Equation 2 was chosen over other electric double layer models because it (a) is applicable to the interfacial potential range covered in these experiments, (b) avoids overparameterization, and (c) aids in the comparison of this data to that of our previously published work. Nevertheless, the data were also fit with the triple layer model (TLM), which yielded similar K_{bind} and σ_m values (although the errors associated with these values were large). The results from the TLM analysis are not discussed further in this work.

The initial surface charge densities, σ_0, that were used in the fitting equation were determined in our previous work.[59] The binding constants, K_{bind}, were obtained from the fitting equation (eq 2) and were used to calculate the binding free energies, ΔG_{bind}, with reference to 55.5 M H_2O. Furthermore, in order to calculate the ion density at maximum Mg(II) binding (Figure 1c), we rearranged eq 2 and accounted for oligonucleotide surface coverage (5×10^{11} strands/cm^2) to yield eq 3:

$$n_{ions} = \frac{N_A}{Fz\rho_{DNA}} \left(\left(\frac{\sinh\left[\frac{E_{SHG} - A}{B}\right]}{30.19 \; M^{1/2} \; m^2 \; C^{-1} \sqrt{C_{elec}}} \right) - \sigma_0 \right) \quad (3)$$

where N_A is Avogadro's number, F is Faraday's constant, z is the charge of magnesium (+2), and ρ_{DNA} is the surface coverage of oligonucleotide strands. In our prior work, we reported that under the conditions presented here (10 mM background NaCl, pH 7) magnesium binds as a divalent (+2) ion.[41] Furthermore, ρ_{DNA} was found to be invariant (5×10^{11} strands / cm^2) for the oligonucleotide strand lengths presented here.[59] Lastly, the total binding free energy, ΔG_{total}, was calculated after normalization to the 55.5 M reference state of water from the binding constant as the product of the binding free energy and the corresponding ion density.

D. Atomic Force Microscopy. The oligonucleotide-functionalized substrates were imaged in tapping mode under aqueous conditions using a Bioscope II Scanning Probe Microscope with a NanoScope V controller (Digital Instruments) with a resolution of 512×512 lines. The tips used in all of the AFM experiments described herein were V-shaped SNL-10 probe (Veeco) with a 0.06 N/m spring constant and a 12−24 kHz resonant frequency. All of the images were collected under the same conditions (10 mM NaCl, pH 7) as the previously described SHG experiments. Initially, large images (1 μm × 1 μm) were taken at 2 Hz. The scan size was then reduced to 333 nm × 333 nm, and the scan rate was decreased to 1 Hz. Images were taken of three to four different spots on a single substrate. A sample 333 nm × 333 nm AFM image without Mg(II) present can be found in Figure 1d. The 10 mM NaCl solution was then pipetted off of the surface and replaced

with a 10 mM NaCl/3 mM $MgCl_2$ solution (Figure 1e). This $MgCl_2$ concentration was selected because in the SHG experiments, it was found to represent a concentration regime associated with maximum metal adsorption (Supporting Information). The samples were reimaged with this concentration using the same protocol as described above. This experiment was carried out in duplicate with varied substrates to ensure repeatability. All images were third-order flattened and low-pass filtered. AFM images were loaded into an Igor Pro software program and converted into a matrix of height profiles to be analyzed in a histogram format (number of bins = 30, bin width = 1). Each histogram contains only the data from one substrate (although multiple spots within that substrate), imaged the same day and with the same tip, in order to prevent variations in different AFM tips from affecting the height profiles between data contained in the histograms (Figure 1f).

III. RESULTS AND DISCUSSION

A. Magnesium Binding as a Function of Strand Length. Figures 2a and 2b show the $|\Delta G_{bind}|$ and ion densities as a function of strand length for both adenine and guanine
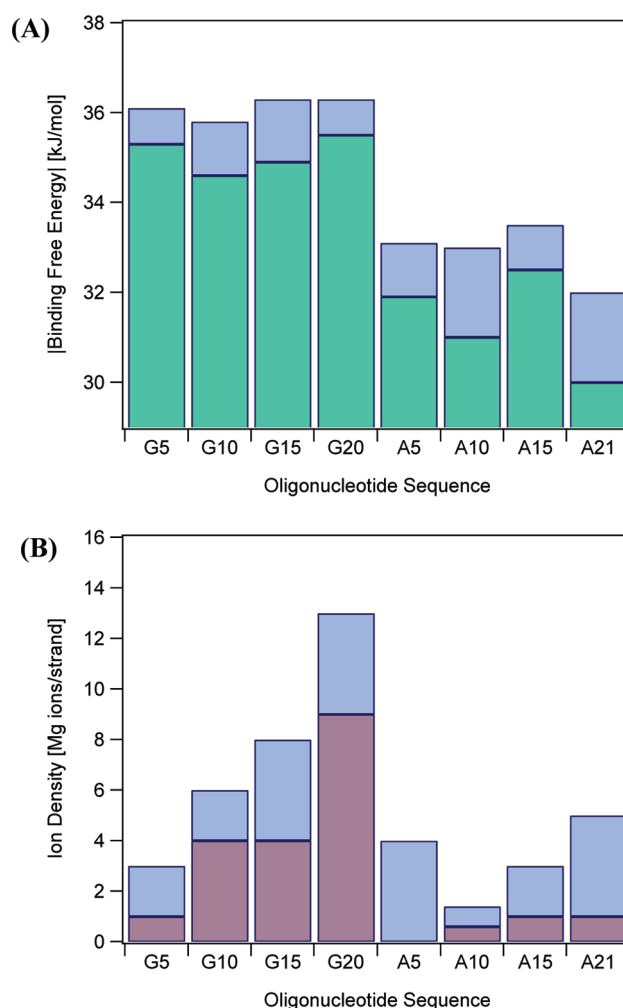

Figure 2. (A) Free energies of binding (kJ/mol) as a function of strand length. (B) Ion densities (Mg/strand) as a function of strand length. All experiments were performed at 298 K, pH 7, 10 mM NaCl. Please note: the blue bars indicate the range of the error.

oligonucleotides, while the results of the corresponding $\chi^{(3)}$ adsorption/desorption studies are shown in Table S1 of the Supporting Information. Figure 2a shows the ΔG_{bind} is invariant with strand length for both adenine and guanine oligomers and is averaged to be −32.1(4) and −35.6(2) kJ/mol, respectively. The number in parentheses corresponds to the uncertainty within that significant figure, i.e., 32.1(4) means 32.1 ± 0.4. This is not surprising as previous results assert that the binding constant represents the affinity of one metal ion to one binding site (K_{bind} is mol^{-1} of binding sites). Therefore, regardless of how many ions or nucleotides are present, the fundamental interaction will be the same to zero-order approximation and assuming other physical conditions such as NaCl concentration, pH, and temperature are held constant. These results coincide with findings from bulk measurements that show that adenine is a weaker binder than guanine.[48,53,71,72] The lack of length dependency corroborates our earlier published findings that suggest the difference in free energies are due to variations in electron density of these surface-bound nucleobases.[42]

Figure 2b shows that the number of Mg(II) ions bound depends linearly on guanine strand length. This linearity corresponds to approximately 80−120% of the negative charges on the phosphate backbone being screened over the range of strands studied. In contrast, the Mg(II) ion density does not increase linearly with adenine strand length but stays, on average, around 2(1) ions/strand. This constant ion density results in approximately 80% and 30% of the negative phosphate charges being screened for a 5-mer and 21-mer, respectively.

Multiplying the number of bound Mg(II) ions to the guanine oligomers with the corresponding free binding energy yields the total free energy of binding for Mg(II) to guanine oligomers, which ranges from −70(40) to −400(70) kJ/mol, while the average total free energy of binding for Mg(II) to adenine oligomers is found to be −70(20) kJ/mol. These results reveal that it is not simply the number of phosphate groups present on a given oligomer that determines the ion density. We hypothesize that the differences in ion densities are attributed to either (a) changes in the structure of the strands resultant from adsorption of Mg(II) ions or (b) disparity of free energies of binding, which results in a more even distribution of Mg(II) ions over the oligomer.

B. Predicting Binding Free Energies for Mixed Strands. It is desirable to move beyond an empirical understanding of the interactions studied here and toward a predictive parameter-based understanding. From a first-order approximation (i.e., excluding cross-terms that describe potential synergistic, structural, etc., contributions), our work above provides a basis for predicting the binding free energies of Mg(II) ions to mixed oligomer systems of guanine and adenine oligonucleotides. We derive our predictions by calculating ΔG_{total} for the mixed strands from the known surface-specific ΔG_{bind} and ion density values of the homo-oligomers over the range of oligomer lengths, coupled with the assumption that the ion density of mixed strands will act in a strictly additive function. We calculate the ΔG_{total} for mixed strands in the following manner:

$$\Delta G_{total} = (\rho_{length}^{Adenine} \Delta G_{bind}^{Adenine}) + (\rho_{length}^{Guanine} \Delta G_{bind}^{Guanine}) \quad (4)$$

We propose that this method can be used to calculate the ΔG_{total} values for mixed strands of adenine and guanine up to 40-mer in length (20 A and 20 G residues). As an example, we

have compiled the matrix for a mixed sequence of 10 A and 10 G residues (Figure 3). For the mixed 20-mer of residues, we
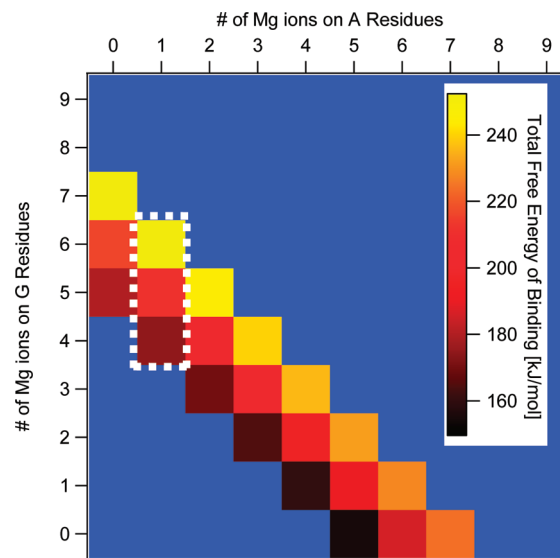

Figure 3. ΔG_{total} (kJ/mol) calculated for mixed strands of guanine and adenine residues at pH 7, 298 K, 10 mM NaCl, and at maximum Mg(II) binding. The weight dashed box indicates the experimental results for a 20-mer of 10 A and 10 G residues binding 1.0(4) and 5(1) Mg(II) ions, respectively.
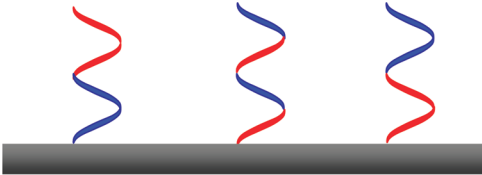
predict (based on the length-dependent studies) the range of the total number of Mg(II) ions bound to be 5−7. From Figure 2b, we know a 10-mer of adenines can have a maximum loading of 1.0(4) Mg(II) ions; thus, the predicted ΔG_{total} values must fall within the bounds of the dashed white box. This restricts the predicted values to −248 to −175 kJ/mol.

C. Magnesium Binding to Mixed Oligomers. Equation 4 neglects the role of sequence order, which may be important for surface-bound oligonucleotides. Thus, it was necessary to determine the efficacy and limits of this equation by experimentally determining the ΔG_{total} values of mixed oligomers. To this end, we studied 20-mer strands of 5′-G$_{10}$A$_{10}$-3′, 5′-A$_{10}$G$_{10}$-3′, and 5′-(AG)$_{10}$-3′ (in which the -3′ end is covalently attached to the surface via the linker). Leading up to these experiments, structural questions arose on how the binding parameters for mixed strands, such as K_{bind}, ΔG_{bind}, ion density, and ΔG_{total}, would differ based on nucleobase accessibility, i.e., whether guanine (with a higher free energy of binding and ion density) is more or less accessible (closer to the bulk solution) relative to the position of adenine (the weaker-binding nucleobase). Accessibility may play a role if the strands vertically extend from the surface into the bulk aqueous solution. Furthermore, it is reasonable to assume that vertically extended oligomers have different binding energies and metal ion densities from randomly coiled strands or strands arranged in a less accessible structure. In order to understand the roles that oligonucleotide sequence order and extension play in our predictions, we employed SHG and AFM.

The adsorption/desorption $\chi^{(3)}$ experiments performed for the 5′-G$_{10}$A$_{10}$-3′, 5′-A$_{10}$G$_{10}$-3′, and 5′-(AG)$_{10}$-3′ oligomers were identical in design to those previously described. The isotherms were fit by substituting for Φ_o in eq 1 with the Langmuir isotherm-modified Gouy−Chapman equation (eq 2). All three mixed oligonucleotide strands yielded roughly the same K_{bind} (Supporting Information Table 2). Because the σ_m, ion

densities, and ΔG_{total} obtained from the fits are associated with large uncertainties, we refit the isotherms by holding K_{bind} constant as the average of the three mixed strand K_{bind} values (1.3×10^4 M^{-1}). This substantially decreased the uncertainties in the ion densities and ΔG_{total} (Table 1).

Table 1. Free Energies of Binding, Ion Number Densities, and Total Free Binding Energies for Mg(II) Binding to $G_{10}A_{10}$, $(AG)_{10}$, and $A_{10}G_{10}$ Fused Silica/Water Interfaces at 298 K, pH 7, and 10 mM NaCl Concentration[a]

	$G_{10}A_{10}$	$(AG)_{10}$	$A_{10}G_{10}$
Order (from bulk)	STRONG-WEAK	MIXED	WEAK-STRONG
ΔG_{bind} [kJ/mol]	-33(1)	-33(1)	-33(1)
Ion Density [ions/strand]	3(1)	4(2)	8(2)
ΔG_{total} [kJ/mol]	-100(30)	-130(70)	-270(70)

[a] Free energies were calculated after referencing to the 55.5 molarity of water, ion densities were calculated by using eq 3, and total free binding energies are the product of free energies of binding and ion densities.

The ΔG_{bind} values for the three mixed oligonucleotides presented in Table 1 represent the average of the ΔG_{bind} values reported in the previous section for the G and A homo-oligomers. The per-site free energy of binding indicates that Mg(II) is binding to either G or A sites or both. While ΔG_{bind} is invariant with the nucleobase sequence, the ion density is not. Table 1 shows that when G residues are furthest from the surface, as is the case for $G_{10}A_{10}$, the lowest number of Mg(II) ions are bound. Conversely, when guanine residues are the closest to the surface, as is the case for $A_{10}G_{10}$, the highest number of Mg(II) ions are bound per strand. The $(AG)_{10}$ strand serves as the median between the $A_{10}G_{10}$ and $G_{10}A_{10}$ strands.

Comparing our experimental results (Table 1) to the predicted values (Figure 3) that were calculated from our additive eq 4, we find that only the experimental results for the strands $(AG)_{10}$ and $A_{10}G_{10}$ fall within the predicted bounds (-248 to -175 kJ/mol) for total free binding energy. This finding suggests that Mg(II) interactions with $(AG)_{10}$ and $A_{10}G_{10}$ strands are best described by an additive approach, such as that presented in eq 4. The fact that the experimentally determined and calculated free energy values for the $G_{10}A_{10}$ strand are at variance suggests that the interaction of Mg(II) with this particular strand is neither additive nor synergistic. This result highlights the importance for addressing issues of sequence order relative to the surface for increasingly complex future models.

D. Atomic Force Microscopy. From the results shown in Table 1, it is not immediately obvious why the lowest number of Mg(II) ions are bound when the strongest nucleobase is

positioned furthest from the surface, as is presumably the case for $G_{10}A_{10}$. When the stronger binding guanine bases are closest to the bulk aqueous phase, one would expect more ions to be bound per strand; however, as the experimental results reveal, this is not the case. In order to determine if changes in the height profiles of mixed oligomer strands explain the results presented in Table 1, AFM images were analyzed as described in Experimental section D. Tapping mode images were obtained and analyzed in the absence and presence of 3 mM MgCl$_2$ which corresponded to the maximum ion density in the SHG $\chi^{(3)}$ experiments (Supporting Information). The height histograms shown in Figures 4a, 4b, and 4c correspond to the height profiles analyzed for $G_{10}A_{10}$, $(AG)_{10}$, and $A_{10}G_{10}$, respectively. We find that the only mixed oligomer which showed a decrease in height upon Mg(II) binding was $A_{10}G_{10}$ (Figure 4c). This strand corresponded to the highest relative ion density (8 ± 2 ions/strand). AFM results show the height of $A_{10}G_{10}$ strands decrease by ~16% that upon Mg(II) binding. A similar decrease in oligonucleotide height following metal ion binding to 40-mers of thymine was previously described by us using results garnered from AFM and sum frequency generation (SFG).[27] In that work, the decrease in height was attributed to the specific binding of Mg ions and not simply to changes in ionic strength, which subsequently screened the Coulombic repulsions present because of the negatively charged phosphate backbone of DNA.[27] Furthermore, controlled studies concluded that the NHS linker does not play an appreciable role in influencing the structural changes.[27]

Because the global minimum may change substantially based on the presence of surface defects, we restrict the discussion of these strands to the relative height profiles, which allows for a comparison of the histograms pre- and post-Mg(II) binding. From this analysis, we find that the $G_{10}A_{10}$ or $(AG)_{10}$ strands show a negligible change in height following Mg(II) binding (Figure 4a,b). The low Mg(II) ion densities for these two strands, which correspond to just 30(10)% and 40(20)% of the charges on the strands, are not enough to collapse them via screening of the Coulombic potentials. This suggests that relatively high ion densities must be reached before the strands studied here collapse in on themselves. Indeed, a collapse is observed for the $A_{10}G_{10}$ strand, which exhibits a Mg(II) ion density that corresponds to 80(20)% of the negative phosphate charges.

We propose that the differences in ion densities for mixed strands of varying sequence order could be due to the relative affinities of the Mg(II) ions to the adenine and guanine bases and to the accessibility of each nucleotide to Mg(II). If guanine and adenine, which have very different binding affinities toward Mg(II), were lying flat at the interface, they would both be equally accessible, and the differences in Mg(II) loading would probably be minor. Instead, the finding that the $A_{10}G_{10}$ strand, in which the strongly binding guanine residues are located near the 3' end that is covalently attached to the fused silica substrate, binds by far the most Mg(II) ions suggests that the spatial arrangement of the residues may not be equal. This hypothesis is graphically depicted in Figure 4d, which shows that Mg(II) ions may bypass the weakly binding adenine residues located near the bulk aqueous phase and coordinate to the strongly binding guanine residues, which are located closer to the surface in this cartoon. In this scenario, the $A_{10}G_{10}$ strand fills from the bottom up, resulting in an oligomer with more evenly distributed charge and thus higher ion density. G-quadruplex formation[73−76] could be important as well in this
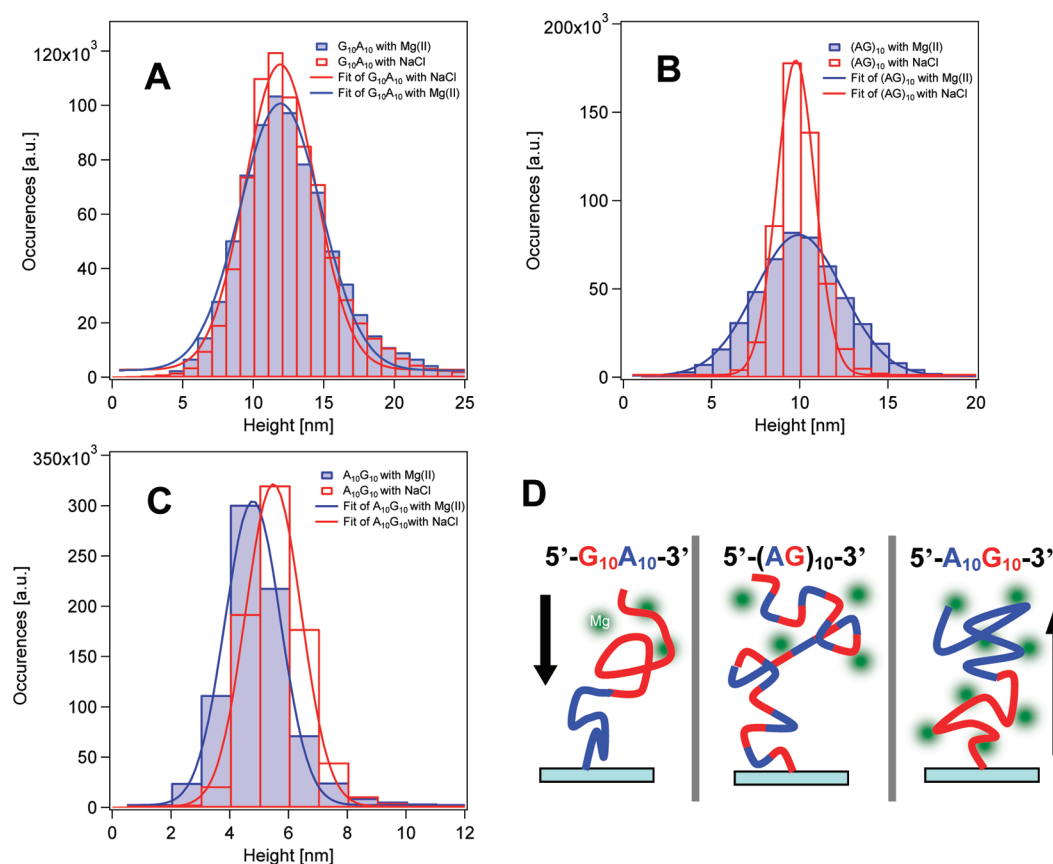
Figure 4. Histogram analysis of aqueous tapping mode AFM images of (a) $G_{10}A_{10}$, (b) $(AG)_{10}$, and (c) $A_{10}G_{10}$, with and without 3 mM $MgCl_2$ at 298 K, pH 7, 10 mM NaCl. (d) Cartoon depiction of proposed possible variations in structure and ion density for the $G_{10}A_{10}$, $A_{10}G_{10}$, and the $(AG)_{10}$ sequences. The gray circles represent Mg(II) ions, the red line represents guanine residues, the blue line represents adenine residues, and the arrows represent the direction of ion loading.

scenario, but we are not aware of whether Mg(II) could form such structures at interfaces. In this scenario, after initially binding of Mg(II) ions to the quadruplex, additional Mg(II) ions may be prevented either electrostatically (as described above) or sterically from docking at the preferred binding site, resulting in a low overall ion density. For the case of $G_{10}A_{10}$, the ions may "bunch up" on the strongly binding guanine residues which are now located closest to the bulk solution. The resulting high density of positive charge near the strand end close to the bulk water may repel subsequent ions from making their way to the adenine residues located closer to the surface (Figure 4d). We conclude that the spatial preference of Mg(II) binding to the $G_{10}A_{10}$ or $A_{10}G_{10}$ strands is biased in opposite directions. Because of the alternating nature of the $(AG)_{10}$ strand, guanine residues are available for binding in the upper half of the strand, and thus Mg(II) loading is identical to that of the $G_{10}A_{10}$ strand.

IV. CONCLUSIONS

In conclusion, we have studied the binding of Mg(II) ions to surface-bound single-stranded oligonucleotides using SHG and AFM. The effect of strand length on Mg(II) ion density and free energy of binding was examined for 5-, 10-, 15-, and 20-mers of adenine and guanine as well as mixed 20-mers of adenine and guanine, at pH 7, 298 K, and 10 mM NaCl. The results for the strand-length dependence are consistent with the notion that the ΔG_{bind} is invariant with strand length for both adenine and guanine oligomers and is averaged to be $-32.1(4)$

and $-35.6(2)$ kJ/mol, respectively. The results also reveal that differences in ion densities are not exclusively dependent on the number of phosphate groups present on a given oligomer; rather, changes in the structure of the strands, which result from disparities in the adsorption free energy of Mg(II) ions, are the primary contributors to determining the number density and distribution of Mg(II) ions over the oligomer. Furthermore, the results from the strand-length-dependent studies serve as the starting place for predicting the total free energy of binding for mixed oligomer strands. While the additive approach discussed does not take structural, synergistic, or subtractive principles into account, it exists as a starting place from which more complex models may be built. Lastly, both the SHG and AFM results for the mixed oligomers of adenine and guanine suggest that ion density is biased through the availability (or lack, thereof) of strongly binding guanine residues located near the bulk aqueous phase.

The insight into Mg(II) binding to surface-localized oligonucleotides presented here sheds important light upon the nature of metal/nucleotide interactions in general and serves as a useful complement to studies involving surface-bound aptamers, which can be highly selective and powerful metal ion binders if they possess the right sequence, which is often only found through combinatorial library approaches. A comprehensive picture of how strand length and heterogeneity affects metal ion/oligonucleotide interactions will be important for developing predictive capabilities for the *de novo* design of aptamers for specific targets. Such an approach has the potential

to make the discovery-based approaches that are currently used for these purposes more efficient. Future work will examine the role that the counterions play and center on the implications of oligonucleotide surface packing density on metal ion binding. Lastly, combining SHG microscopy with existing nano-lithography techniques as a high-throughput way of studying and characterizing these model interfaces would be extremely advantageous.

■ ASSOCIATED CONTENT

Ⓢ Supporting Information

Individual adsorption isotherms, additional AFM histograms, and table of results from Mg binding as a function of strand length. This material is available free of charge via the Internet at http://pubs.acs.org.

■ AUTHOR INFORMATION

Corresponding Author

*E-mail: geigerf@chem.northwestern.edu.

Notes

The authors declare no competing financial interest.

■ ACKNOWLEDGMENTS

■ REFERENCES

(1) Draper, D. E.; Grilley, D.; Soto, A. M. *Annu. Rev. Biophys. Biomol. Struct.* **2005**, *34*, 221–243.

(2) Record, M. T. *Biopolymers* **1975**, *14*, 2137–2158.

(3) Sines, C. C.; McFail-Isom, L.; Howerton, S. B.; VanDerveer, D.; Williams, L. D. *J. Am. Chem. Soc.* **2000**, *122*, 11048–11056.

(4) Davey, C. A.; Richmond, T. J. *Proc. Natl. Acad. Sci. U. S. A.* **2002**, *99*, 11169–11174.

(5) Dobi, A.; v. Agoston, D. *Proc. Natl. Acad. Sci. U. S. A.* **1998**, *95*, 5981–5986.

(6) Cowan, J. A.; Pingoud, A. M. Springer: Berlin, 2004; Vol. *14*, pp 339–360.

(7) DeHaseth, P. L.; Lohman, T. M.; Record, M. T. *Biochemistry* **1977**, *16*, 4783–4790.

(8) Wu, F. Y. H.; Wu, C. W. *Annu. Rev. Nutr.* **1987**, *7*, 251–272.

(9) Ghosh, A.; Ginty, D. D.; Bading, H.; Greenberg, M. E. *J. Neurobiol.* **1994**, *25*, 294–303.

(10) Kunkel, T. A.; Loeb, L. A. *J. Biol. Chem.* **1979**, *254*, 5718–5725.

(11) Liu, J.; Cao, Z.; Lu, Y. *Chem. Rev.* **2009**, *109*, 1948–1998.

(12) Liu, J.; Brown, A. K.; Meng, X.; Cropek, D. M.; Istok, J. D.; Watson, D. B.; Lu, Y. *Proc. Natl. Acad. Sci. U. S. A.* **2007**, *104*, 2056–2061.

(13) Cho, E. J.; Lee, J.-W.; Ellington, A. D. *Annu. Rev. Anal. Chem.* **2009**, *2*, 241.

(14) Dalavoy, T. S.; Wernette, D. P.; Gong, M.; Sweedler, J. V.; Lu, Y.; Flachsbart, B. R.; Shannon, M. A.; Bohn, P. W.; Cropek, D. M. *Lab Chip* **2008**, *8*, 786.

(15) Tombelli, S.; Minunni, M.; Mascini, M. *Biosens. Bioelectron.* **2005**, *20*, 2424–2434.

(16) D'Orazio, P. *Clin. Chim. Acta* **2003**, *334*, 41–69.

(17) Wan, Y.; Kim, Y.-t.; Li, N.; Cho, S. K.; Bachoo, R.; Ellington, A. D.; Iqbal, S. M. *Cancer Res.* **2010**, *70*, 9371–9380.

(18) Lautner, G.; Balogh, Z.; Bardoczy, V.; Meszaros, T.; Gyurcsanyi, R. E. *Analyst* **2010**, *135*, 918–926.

(19) Mirkin, C. A.; Letsinger, R. L.; Mucic, R. C.; Storhoff, J. J. *Nature* **1996**, *382*, 607–609.

(20) Seeman, N. C. *Nature* **2003**, *421*, 427–431.

(21) Wang, X.; Liu, F.; Wang, K. L.; Ozkan, C. S. *J. Nanoelectron. Optoelectron.* **2006**, *1*, 203–210.

(22) Le, J. D.; Pinto, Y.; Seeman, N. C.; Musier-Forsyth, K.; Taton, T. A.; Kiehl, R. A. *Nano Lett.* **2004**, *4*, 2343–2347.

(23) Lee, J. F.; Hesselberth, J. R.; Meyers, L. A.; Ellington, A. D. *Nucleic Acids Res.* **2004**, *32*, D95–D100.

(24) Stoltenburg, R.; Reinemann, C.; Strehlitz, B. *Biomol. Eng.* **2007**, *24*, 381–403.

(25) *The Aptamer Handbook: Functional Oligonucleotides and Their Application*; Klussmann, S., Ed.; John Wiley & Sons: San Francisco, CA, 2006.

(26) Shangguan, D.; Li, Y.; Tang, Z.; Cao, Z. C.; Chen, H. W.; Mallikaratchy, P.; Sefah, K.; Yang, C. J.; Tan, W. *Proc. Natl. Acad. Sci. U. S. A.* **2006**, *103*, 11838–11843.

(27) Walter, S. R.; Holland, J. G.; Gieseck, R. L.; Geiger, F. M. 2012, submitted for publication.

(28) Howell, C.; Schmidt, R.; Kurz, V.; Koelsch, P. *Biointerphases* **2008**, *3*, FC47–FC51.

(29) Asanuma, H.; Noguchi, H.; Uosaki, K.; Yu, H.-Z. *J. Am. Chem. Soc.* **2008**, *130*, 8016–8022.

(30) Casero, E.; Darder, M.; Diaz, D. J.; Pariente, F.; Martin-Gago, J. A.; Abruna, H.; Lorenzo, E. *Langmuir* **2003**, *19*, 6230–6235.

(31) Wu, N.; Zhou, X.; Czajkowsky, D. M.; Ye, M.; Zeng, D.; Fu, Y.; Fan, C.; Hu, J.; Li, B. *Nanoscale*, *3*.

(32) Onoa, G. B.; Cervantes, G.; Moreno, V.; Prieto, M. J. *Nucleic Acids Res.* **1998**, *26*, 1473–1480.

(33) Hansma, H. G.; Bezanilla, M.; Zenhausern, F.; Adrian, M.; Sinsheimer, R. L. *Nucleic Acids Res.* **1993**, *21*, 505–512.

(34) Sartenaer, Y.; Tourillon, G. r.; Dreesen, L.; Lis, D.; Mani, A. A.; Thiry, P. A.; Peremans, A. *Biosens. Bioelectron.* **2007**, *22*, 2179–2183.

(35) Zhao, X.; Subrahmanyan, S.; Eisenthal, K. B. *Chem. Phys. Lett.* **1990**, *171*, 558.

(36) Hayes, P. L.; Malin, J. N.; Jordan, D. S.; Geiger, F. M. *Chem. Phys. Lett.* **2010**, *499*, 183–192.

(37) Wolf, F. I.; Cittadini, A. *Mol. Aspects Med.* **2003**, *24*, 3–9.

(38) Anastassopoulou, J.; Theophanides, T. *Crit. Rev. Oncol./ Hematol.* **2002**, *42*, 79–91.

(39) MacKerell, A. D. *J. Phys. Chem. B* **1997**, *101*, 646–650.

(40) Hartwig, A. *Mutat. Res., Fundam. Mol. Mech. Mutagen.* **2001**, *475*, 113–121.

(41) Holland, J. G.; Jordan, D. S.; Geiger, F. M. *J. Phys. Chem. B* **2011**, *115*, 8338–8345.

(42) Holland, J. G.; Malin, J. N.; Jordan, D. S.; Morales, E.; Geiger, F. M. *J. Am. Chem. Soc.* **2011**, *133*, 6098–6098.

(43) Chiu, T. K.; Dickerson, R. E. *J. Mol. Biol.* **2000**, *301*, 915–945.

(44) Clement, R. M.; Sturm, J.; Daune, M. P. *Biopolymers* **1973**, *12*, 405–421.

(45) Duguid, J.; Bloomfield, V. A.; Benevides, J.; Thomas, G. J., Jr. *Biophys. J.* **1993**, *65*, 1916–1928.

(46) Duguid, J. G.; Bloomfield, V. A.; Benevides, J. M.; Thomas, G. J., Jr. *Biophys. J.* **1995**, *69*, 2623–2641.

(47) Hackl, E. V.; Kornilova, S. V.; Kapinos, L. E.; Andrushchenko, V. V.; Galkin, V. L.; Grigoriev, D. N.; Blagoi, Y. P. *J. Mol. Struct.* **1997**, *408–409*, 229–232.

(48) Solt, I.; Simon, I.; Csaszar, A. G.; Fuxreiter, M. *J. Phys. Chem. B* **2007**, *111*, 6272–6279.

(49) Misra, V. K.; Draper, D. E. *J. Mol. Biol.* **1999**, *294*, 1135−1147.

(50) Gessner, R. V.; Frederick, C. A.; Quigley, G. J.; Rich, A.; Wang, A. H. *J. Biol. Chem.* **1989**, *264*, 7921−7935.

(51) Gessner, R. V.; Quigley, G. J.; Wang, A. H. J.; Van der Marel, G. A.; Van Boom, J. H.; Rich, A. *Biochemistry* **1985**, *24*, 237−240.

(52) Subirana, J. A.; Soler-Lopez, M. *Annu. Rev. Biophys. Biomol. Struct.* **2003**, *32*, 27−45.

(53) Cowan, J. A.; Huang, H. W.; Hsu, L. Y. *J. Inorg. Biochem.* **1993**, *52*, 121−129.

(54) Maguire, M. E.; Cowan, J. A. *BioMetals* **2002**, *15*, 203−210.

(55) Kankia, B. I. *Biopolymers* **2004**, *74*, 232−239.

(56) Kankia, B. I. *Biophys. Chem.* **2003**, *104*, 643−654.

(57) Eichhorn, G. L.; Shin, Y. A. *J. Am. Chem. Soc.* **1968**, *90*, 7323−7328.

(58) Holland, J. G.; Malin, J. N.; Jordan, D. S.; Geiger, F. M. *J. Am. Chem. Soc.* **2011**, *133*, 2567−2570.

(59) Boman, F. C.; Gibbs-Davis, J. M.; Heckman, L. M.; Stepp, B. R.; Nguyen, S. T.; Geiger, F. M. *J. Am. Chem. Soc.* **2009**, *131*, 844−848.

(60) Boman, F. C.; Musorrafiti, M. J.; Gibbs, J. M.; Stepp, B. R.; Salazar, A. M.; Nguyen, S. T.; Geiger, F. M. *J. Am. Chem. Soc.* **2005**, *127*, 15368−15369.

(61) Hayes, P. L.; Malin, J. N.; Konek, C. T.; Geiger, F. M. *J. Phys. Chem. A* **2008**, *112*, 660−668.

(62) Malin, J. N.; Hayes, P. L.; Geiger, F. M. *J. Phys. Chem. C* **2009**, *113*, 2041−2052.

(63) Hayes, P. L.; Gibbs-Davis, J. M.; Musorrafiti, M. J.; Mifflin, A. L.; Scheidt, K. A.; Geiger, F. M. *J. Phys. Chem. C* **2007**, *111*, 8796−8804.

(64) Mifflin, A. L.; Musorrafiti, M. J.; Konek, C. T.; Geiger, F. M. *J. Phys. Chem. B* **2005**, *109*, 24386−24390.

(65) Malin, J. N.; Geiger, F. M. *J. Phys. Chem. A* **2010**, *114*, 1797−1805.

(66) Malin, J. N.; Holland, J. G.; Geiger, F. M. *J. Phys. Chem. C* **2009**, *113*, 17795−17802.

(67) Al-Abadleh, H. A.; Voges, A. B.; Bertin, P. A.; Nguyen; Geiger, F. M. *J. Am. Chem. Soc.* **2004**, *126*, 11126−11127.

(68) Jordan, D. S.; Malin, J. N.; Geiger, F. M. *Environ. Sci. Technol.* **2010**, *44*, 5862−5867.

(69) Holland, J. G.; Malin, J. N.; Jordan, D. S.; Morales, E.; Geiger, F. M. *J. Am. Chem. Soc.* **2011**, *133*, 6098−6098.

(70) Stumm, W.; Morgan, J. J. *Aquatic Chemistry*, 3rd ed.; John Wiley & Sons, Inc.: New York, 1996.

(71) *Metal Ion in Biological Systems: Interactions of Metal Ions with Nucleotides, Nucleic Acids and Their Constituent*; Sigel, A., Sigel, H., Eds.; Marcel Dekker: New York, 1996; Vol. 32.

(72) Li, W.; Nordenskiold, L.; Mu, Y. *J. Phys. Chem. B* **2011**, *115*, 14713−14720.

(73) Poon, K.; Macgregor, R. B. *Biopolymers* **1998**, *45*, 427−434.

(74) Kankia, B. I.; Marky, L. A. *J. Am. Chem. Soc.* **2001**, *123*, 10799−10804.

(75) Kotch, F. W.; Fettinger, J. C.; Davis, J. T. *Org. Lett.* **2000**, *2*, 3277−3280.

(76) Shi, X.; Fettinger, J. C.; Davis, J. T. *J. Am. Chem. Soc.* **2001**, *123*, 6738−6739.